



## A node-based smoothed point interpolation method (NS-PIM) for three-dimensional heat transfer problems

S.C. Wu<sup>a,b,\*</sup>, G.R. Liu<sup>b,c</sup>, H.O. Zhang<sup>a</sup>, X. Xu<sup>c,d</sup>, Z.R. Li<sup>c</sup>

<sup>a</sup> State Key Laboratory of Digital Manufacturing and Equipment Technology, Huazhong University of Science and Technology, Wuhan, 430074, P.R. China

<sup>b</sup> Centre for Advanced Computations in Engineering Science (ACES), Department of Mechanical Engineering, National University of Singapore, 9 Engineering Drive 1, 117576 Singapore

<sup>c</sup> Singapore-MIT Alliance (SMA), E4-04-10, 4 Engineering Drive 3, 117576 Singapore

<sup>d</sup> College of Mathematics, Jinlin University, 2699 Qianjin Street, Changchun, 130012, P.R. China

### ARTICLE INFO

#### Article history:

Received 22 February 2008

Received in revised form 4 August 2008

Accepted 30 October 2008

Available online 22 November 2008

#### Keywords:

Meshfree

Gradient smoothing

Solution bounds

Point interpolation method

Three-dimensional heat transfer

### ABSTRACT

A node-based smoothed point interpolation method (NS-PIM) is formulated for three-dimensional (3D) heat transfer problems with complex geometries and complicated boundary conditions. Shape functions constructed here through PIM possess the delta function property and hence allow the straightforward enforcement of essential boundary conditions. The smoothed Galerkin weak form is employed to create discretized system equations, and the node-based smoothing domains are used to perform the smoothing operation and the numerical integration. The accuracy and efficiency of the NS-PIM solutions are studied through detailed analyses of actual 3D heat transfer problems. It is found that the NS-PIM can provide higher accuracy in temperature and its gradient than the reference approach does, in which very fine meshes are used in standard FEM code available with homogeneous essential boundary conditions. More importantly, the upper bound property of the NS-PIM is obtained using the same tetrahedral mesh. Together with the FEM, we now have a simple means to obtain both upper and lower bounds of the exact solution to heat transfer using the same type of mesh.

Crown Copyright © 2008 Published by Elsevier Masson SAS. All rights reserved.

### 1. Introduction

Finite element method (FEM) [1] has been widely used to solve various types of practical problems of engineering and sciences. However, FEM has some inherent drawbacks due to its strong reliance on the element mesh. Recently, meshfree methods have been developed to circumvent some of the problems and have achieved remarkable progress [2,3]. Examples of meshfree methods include the smoothed particle hydrodynamic method (SPH) [4], the element-free Galerkin method (EFG) [5], the reproducing kernel particle method (RKPM) [6], the meshless local Petrov–Galerkin method (MLPG) [7] and the point interpolation method (PIM) [8], etc.

The PIM is a mesh-free approach based on the Galerkin weak form, in which shape functions are constructed to ensure passing through the nodal values exactly at each node arbitrarily scattered within a local support domain. Currently, two types of shape functions have been developed and used widely, including polynomial PIM shape functions [8] and radial PIM shape functions (RPIM) [9, 10]. The PIM shape functions so constructed possess the Delta

function property, which permits the straightforward imposition of point-based loads and node-based essential boundary conditions. By using the nodal integration scheme with strain smoothing proposed by Chen et al. [11], a node-based smoothed PIM (NS-PIM or termed as LC-PIM originally) has been proposed for 2D elasticity and thermoelasticity problems [12,13]. The NS-PIM ensures at least linear consistency and monotonic convergence, and can produce upper bound solutions to the exact solution in energy norm [14]. Compared with linear compatible FEM, NS-PIM works well using the triangular mesh in two dimensions and tetrahedral mesh in three dimensions with better accuracy and higher convergence for mechanics problems [14].

It is well known that the displacement-based fully compatible FEM model always provides a lower bound solution in energy norm for the exact solution to elastic problems [1]. As a very important property, the NS-PIM can give an upper bound solution in energy norm for the problems with homogeneous essential boundary conditions [14]. The combination of NS-PIM and FEM permits one to simply obtain a bounded solution in energy norm to practical problems of complicated geometry, as long as a FEM mesh can be build.

With the increasing interests in applying rapid energy transport systems in manufacturing processes, analysis of complex heat transfer problems with the extreme temperature gradients becomes more and more important [15,16]. Heat induced cracks and

\* Corresponding author at: State Key Laboratory of Digital Manufacturing and Equipment Technology, Huazhong University of Science and Technology, Wuhan, 430074, P.R. China. Tel.: +86 27 87543493; fax: +86 27 87557392.

E-mail address: wushengchuan@gmail.com (S.C. Wu).

**Nomenclature**

$h$	convection coefficient.....	$W/(m^2 \text{ } ^\circ C)$	$\varphi$	PIM shape function
$k_i$	heat conductivity in $x_i$ -direction.....	$W/(m \text{ } ^\circ C)$	$\Gamma$	domain boundary
$\mathbf{k}$	conduction matrix defined in Eq. (17)		$\Pi$	functional operator
$n_i$	the $x_i$ -component of unit outward normal		$\delta$	variational operator
$Q_v$	internal heat source.....	$W/m^3$	$\nabla$	temperature gradient operator
$q_\Gamma$	prescribed heat flux on 2nd boundary		<i>Subscripts</i>	
$\mathbf{q}$	nodal temperature vector		$e$	equivalent energy in Eq. (29)
$T_a$	temperature of ambient medium.....	$^\circ C$	$k$	nodal smoothing domain and volume
$T_\Gamma$	known temperature on 1st boundary.....	$^\circ C$	<i>Superscripts</i>	
$w$	the weighted test function		T	transpose operator
<i>Greek symbols</i>			$h$	convection matrix
$\Phi$	vector of the PIM shape functions			

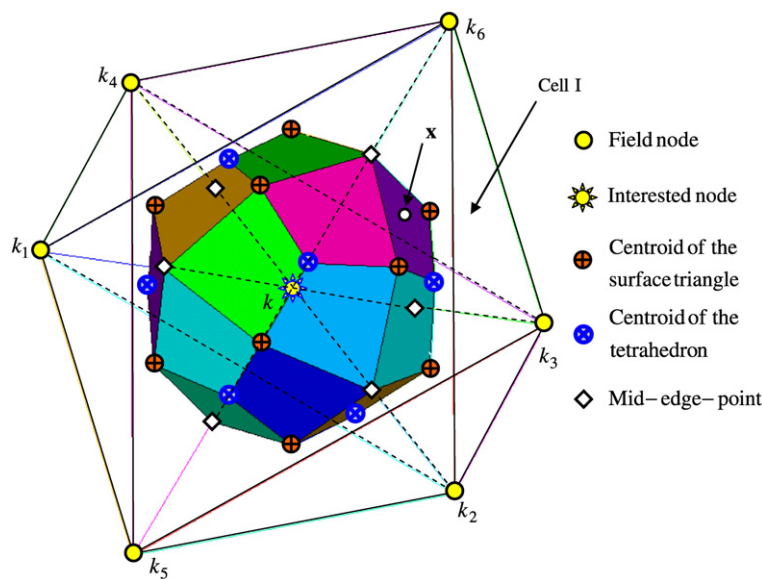


Fig. 1. A typical node-based 3D smoothing domain for node  $k$ .

warps that degrade or even destroy the structures and components are required to accurately predicted [17]. Experimental evaluations of the temperature and its gradient together with the resulted stress are of considerable difficulty for complicated 3D systems. Computational means is therefore usually preferred for studying these kinds of systems. Currently, FEM is widely used for this purpose. However, due to its overly-stiff property of the fully-compatible FEM models, significant errors can occur in the primary variable field especially with high gradient regions. FEMs using assumed strains have been studied to provide more accurate solutions in the gradient of the primary variables. The NS-PIM has also been used to study thermoelastic problems [13], and found to be an excellent alternative to the FEM. It possesses very attractive property in terms of convergence, accuracy and most importantly the upper bound property of numerical solutions. Our results showed that NS-PIM performs well even linear triangular for two dimensions or tetrahedral meshes for three dimensions are used [18], and is desired for evaluating foregoing problems.

This work formulates a NS-PIM for 3D heat transfer problems involving complex geometries and complicated boundary conditions. In the approach, varies types of elements can be used, but we choose to use four-node tetrahedrons as the background cells that can be generated using any standard routine available for 3D solids. PIM shape functions are constructed using polynomial basis and local supporting nodes selected based on the tetrahedron.

Then discretized system equations are derived according to the smoothed Galerkin weak form [18]. Finally, the numerical integration is conducted using the nodal integration procedure [11]. The gradient smoothing technique facilitates the NS-PIM to obtain more accurate temperature and gradient solutions even using the low-order shape functions. The accuracy of numerical solutions are studied in detail and compared with those obtained using the well-developed FEM with the same four-node tetrahedral mesh. We observed the important upper bound property of the present NS-PIM in energy norm for 3D heat transfer problems.

**2. PIM shape functions**

The polynomial point interpolation method is a series representation for meshfree function approximation using a set of arbitrarily distributed nodes inside a local support of an interested point [8]. In the present formulation, the problem domain is firstly discretized with some scattered nodes, and then the background tetrahedrons are formed based on these nodes. Finally, a set of local supports  $\Omega_x$  is constructed using the tetrahedral mesh as sampled shown in Fig. 1.

Consider a field  $u(\mathbf{x})$  defined in this 3D domain  $\Omega_x$  bounded by boundaries  $\Gamma_x$ , it can be approximated using a PIM shape function in the form of

$$u(\mathbf{x}) \approx \Phi^T(\mathbf{x})\mathbf{U}_s \tag{1}$$

where  $\Phi(\mathbf{x})$  are the PIM shape functions that can be expressed as

$$\Phi^T(\mathbf{x}) = \mathbf{P}^T(\mathbf{x})\mathbf{P}_n^{-1} = \{\varphi_1(\mathbf{x}) \quad \varphi_2(\mathbf{x}) \quad \dots \quad \varphi_n(\mathbf{x})\} \quad (2)$$

The derivatives of shape functions can be easily obtained, but they are not required in the present NS-PIM, owing to the use of gradient smoothing technique.

The PIM shape functions are constructed using polynomial or radial function basis [4]. Note that when high order polynomial PIM or RPIM shape functions [9,10] are used, the displacement field is not compatible and the generalized smoothing technique [18] needs to be used. The theoretical foundation for such a formulation should be based on the so-called weakened weak ( $W^2$ ) form that guarantees convergence to the exact solution [19]. In this work, we use only the linear interpolation.

### 3. Discretized system equations

#### 3.1. Smoothed Galerkin weak form

Heat transfer in an anisotropic solid  $\Omega$  bounded by  $\Gamma$  is governed by the following differential equation with a set of boundary conditions

$$k_1 \frac{\partial^2 T}{\partial x^2} + k_2 \frac{\partial^2 T}{\partial y^2} + k_3 \frac{\partial^2 T}{\partial z^2} + Q_v = 0 \quad \Omega \quad \text{Problem domain studied} \quad (3)$$

$$T = T_r \quad \Gamma_1 \quad \text{Dirichlet boundary} \quad (4)$$

$$-n_1 k_1 \frac{\partial T}{\partial x} - n_2 k_2 \frac{\partial T}{\partial y} - n_3 k_3 \frac{\partial T}{\partial z} = q_r \quad \Gamma_2 \quad \text{Neumann boundary} \quad (5)$$

$$-n_1 k_1 \frac{\partial T}{\partial x} - n_2 k_2 \frac{\partial T}{\partial y} - n_3 k_3 \frac{\partial T}{\partial z} = h(T - T_a) \quad \Gamma_3 \quad \text{Robin boundary} \quad (6)$$

where  $k_i$  is the conductivity in  $x_i$ -direction ( $i = 1, 2, 3$ ),  $Q_v$  is the inner energy source,  $n_i$  is  $x_i$ -component of the direction normal,  $T_r$  and  $q_r$  are prescribed temperature and heat flux, respectively,  $h$  is the convection coefficient,  $T_a$  is the temperature of ambient medium.

As the differential equation (3) is satisfied at all points over this problem domain, a weighted residual formulation can be written as:

$$\int_{\Omega} w_k \left[ k_1 \frac{\partial^2 T}{\partial x^2} + k_2 \frac{\partial^2 T}{\partial y^2} + k_3 \frac{\partial^2 T}{\partial z^2} + Q_v \right] d\Omega = 0 \quad (7)$$

where  $w_k$  denotes a set of weighted functions equal in number to the total number of nodes. Due to the fact that the PIM shape functions [8] possess the delta function property, node-based essential boundary conditions can be treated in the same way as in the usual FEM. Applying Green's theorem together with the boundary conditions, the residual form Eq. (7) becomes,

$$\int_{\Gamma_2} w q_r d\Gamma + \int_{\Gamma_3} w h(T - T_a) d\Gamma - \int_{\Omega} w Q_v d\Omega + \int_{\Omega} \left( k_1 \frac{\partial T}{\partial x} \frac{\partial w}{\partial x} + k_2 \frac{\partial T}{\partial y} \frac{\partial w}{\partial y} + k_3 \frac{\partial T}{\partial z} \frac{\partial w}{\partial z} \right) d\Omega = 0 \quad (8)$$

When the PIM shape function is also used as the test function  $w_k$ , we have the following functional for Galerkin formulation

$$\begin{aligned} \Pi(T) = & \int_{\Omega} \frac{1}{2} \left[ k_1 \left( \frac{\partial T}{\partial x} \right)^2 + k_2 \left( \frac{\partial T}{\partial y} \right)^2 + k_3 \left( \frac{\partial T}{\partial z} \right)^2 \right] d\Omega \\ & - \int_{\Omega} T Q_v d\Omega + \int_{\Gamma_2} T q_r d\Gamma + \int_{\Gamma_3} h T \left( \frac{1}{2} T - T_a \right) d\Gamma \end{aligned} \quad (9)$$

Using the variational principle, Eq. (9) reduces to

$$\begin{aligned} \delta \Pi(T) = & \int_{\Omega} \left[ k_1 \frac{\partial T}{\partial x} \delta \frac{\partial T}{\partial x} + k_2 \frac{\partial T}{\partial y} \delta \frac{\partial T}{\partial y} + k_3 \frac{\partial T}{\partial z} \delta \frac{\partial T}{\partial z} \right] d\Omega \\ & - \int_{\Omega} \delta T Q_v d\Omega + \int_{\Gamma_2} \delta T q_r d\Gamma + \int_{\Gamma_3} h T \delta T d\Gamma \\ & - \int_{\Gamma_3} h T_a \delta T d\Gamma \end{aligned} \quad (10)$$

Replaced the temperature gradient presented in Eq. (10) with the smoothed temperature gradient, the smoothed Galerkin weak form for heat transfer problems can be obtained as:

$$\begin{aligned} \int_{\Omega} \delta(\nabla \bar{T})^T \mathbf{k} \nabla \bar{T} d\Omega - \int_{\Omega} \delta T^T Q_v d\Omega + \int_{\Gamma_2} \delta T^T q_r d\Gamma \\ + \int_{\Gamma_3} \delta T^T h T d\Gamma - \int_{\Gamma_3} \delta T^T h T_a d\Gamma = 0 \end{aligned} \quad (11)$$

Substituting Eq. (1) into Eq. (11) and using the arbitrary feature of variations, a set of discretized system equations can be obtained finally in the following matrix form:

$$[\bar{\mathbf{K}} + \mathbf{K}^h] \{\mathbf{q}\} = \{\mathbf{P}\} \quad (12)$$

in which

$$\bar{\mathbf{K}}_{IJ} = \int_{\Omega} \bar{\mathbf{B}}_I^T \mathbf{k} \bar{\mathbf{B}}_J d\Omega \quad (13)$$

$$\mathbf{K}_{IJ}^h = \int_{\Gamma_3} h \Phi_I^T \Phi_J d\Gamma \quad (14)$$

$$\mathbf{P}_I = \int_{\Omega} \Phi_I^T Q_v d\Omega - \int_{\Gamma_2} \Phi_I^T q_r d\Gamma + \int_{\Gamma_3} h T_a \Phi_I^T d\Gamma \quad (15)$$

$$\bar{\mathbf{B}}_I^T = \{\bar{g}_{I1} \quad \bar{g}_{I2} \quad \bar{g}_{I3}\} \quad (16)$$

and

$$\mathbf{k} = \begin{Bmatrix} k_1 & 0 & 0 \\ 0 & k_2 & 0 \\ 0 & 0 & k_3 \end{Bmatrix} \quad (17)$$

where the superscript  $h$  is the convective matrix and  $\mathbf{q}$  the nodal temperature vector.

To evaluate the smoothed stiffness matrix in Eq. (13), node-based smoothing domains are used, and hence the integration is performed also based on nodes, which is detailed in the following section.

#### 3.2. Nodal integration with gradient smoothing

To carry out the integration in Eq. (13), a background mesh of 4-node tetrahedrons with a total number of  $N$  field nodes is first generated. This can be obtained easily using any mesh generator well-developed for FEM. Based on the background tetrahedral mesh, the computation domain  $\Omega$  is divided further into  $N$  smoothing domain of polyhedrons  $\Omega_k$  ( $k = 1, 2, \dots, N$ ) centered by node  $k$ . Fig. 2 is the schematics of a part of a typical nodal smoothing domain. The domain of the smoothing polyhedron for node  $k$

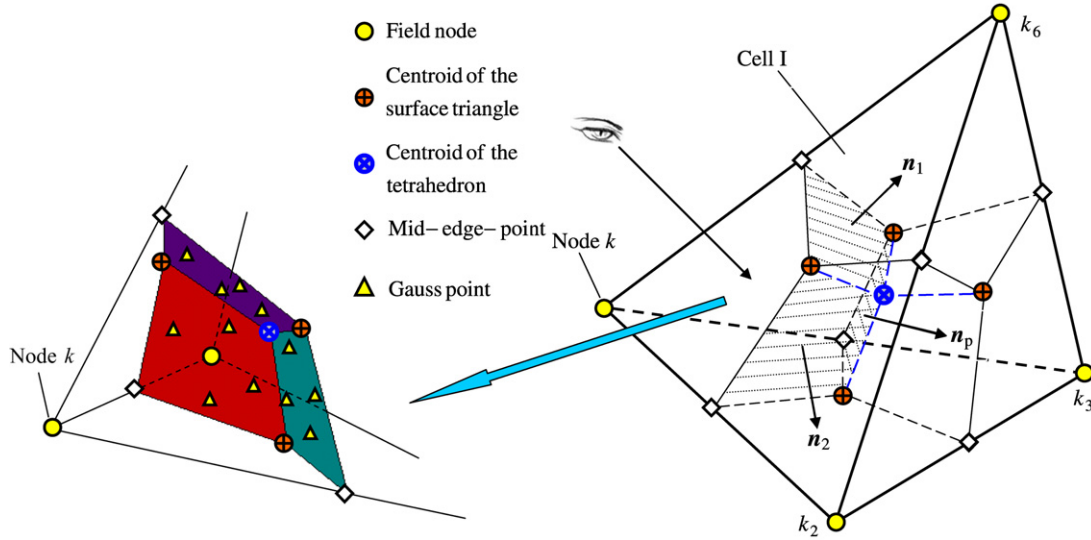


Fig. 2. The schematic of one portion of a node-based smoothing domain for node  $k$  located in a four-node tetrahedral cell  $I$  ( $k$ - $k_2$ - $k_3$ - $k_6$ ).

inside the cell  $I$  is formed by connecting sequentially the mid-edge-points, the centroids of surface triangles, and the centroids of cell  $I$ . The boundary of the smoothing domain  $\Omega_k$  is labeled as  $\Gamma_k$  and the union of all  $\Omega_k$  forms exactly the global domain  $\Omega$ .

Using the nodal integration scheme, the domain integration shown in Eq. (13) can be performed numerically as follows:

$$\bar{\mathbf{K}}_{IJ} = \sum_{k=1}^N \bar{\mathbf{K}}_{IJ}^{(k)} \quad (18)$$

in which the summation implies “assembly”, and

$$\bar{\mathbf{K}}_{IJ}^{(k)} = \int_{\Omega_k} \bar{\mathbf{B}}_I^T \mathbf{k} \bar{\mathbf{B}}_J d\Omega \quad (19)$$

where  $V_k$  is the volume of smoothing domain of node  $k$ .

The generalized gradient smoothing technique that works also for discontinuous field functions [18] is now applied over the smoothing domain to obtain the smoothed nodal gradient for the interested node  $\mathbf{x}_k$

$$\bar{g}_i(\mathbf{x}_k) = \int_{\Omega_k} g_i(\mathbf{x}) W(\mathbf{x} - \mathbf{x}_k) d\Omega \quad (20)$$

where  $g_i$  is the derivative of the field function (temperature) with respect to  $x_i$ , and  $W$  is a smoothing function. For simplicity, a piecewise constant function

$$W(\mathbf{x} - \mathbf{x}_k) = \begin{cases} 1/V_k, & \mathbf{x} \in \Omega_k \\ 0, & \mathbf{x} \notin \Omega_k \end{cases} \quad (21)$$

is used. Note that it is possible to use more sophisticated  $W$  [2] as long as the conditions for smoothing functions are met. However, for problems of complicated geometry, the piecewise constant function is found so far most convenient and resultful to use.

The temperature gradient for node  $k$  and for any point in the smoothing domain is obtained as follows even for discontinuous assumed functions of temperature [18]:

$$\bar{g}_i(\mathbf{x}_k) = \frac{1}{V_k} \int_{\Gamma_k} T n_i d\Gamma \quad (22)$$

which is constant in the smoothing domain  $\Omega_k$ . Using PIM shape functions to construct the field function for temperature, the

smoothed gradient for node  $k$  can be written in the following matrix form

$$\bar{\mathbf{g}}(\mathbf{x}_k) = \sum_{I \in D_k} \bar{\mathbf{B}}_I^{\Omega_k} \mathbf{T}_I \quad (23)$$

where  $D_k$  is the set of all the nodes used in the interpolation for the field function on  $\Gamma_k$ . For three-dimensional spaces, the corresponding forms are given by

$$\bar{\mathbf{g}}^T = \{ \bar{g}_1 \quad \bar{g}_2 \quad \bar{g}_3 \} \quad (24)$$

$$[\bar{\mathbf{B}}_I^{\Omega_k}]^T = [ \bar{b}_{I1} \quad \bar{b}_{I2} \quad \bar{b}_{I3} ] \quad (25)$$

$$\bar{b}_{Ip} = \frac{1}{V_k} \int_{\Gamma_k} \varphi_I(\mathbf{x}) n_p(\mathbf{x}) d\Gamma \quad (p = 1, 2, 3) \quad (26)$$

where  $\varphi_I(\mathbf{x})$  is the PIM shape function for node  $I$ .

Using Gauss integration along each sub-boundary surface  $\Gamma_k$  of the smoothing domain  $\Omega_k$ , Eq. (26) can be rewritten in the following summation forms as

$$\bar{b}_{Ip} = \frac{1}{V_k} \sum_{q=1}^{N_s} \left[ \sum_{r=1}^{N_g} w_r \varphi_I(\mathbf{x}_{qr}) n_p(\mathbf{x}_{qr}) \right] \quad (27)$$

where  $N_s$  is the number of the sub-boundary surface  $\Gamma_k$ ,  $N_g$  is the number of gauss points located in each sub-boundary surface (triangle for global surface, quadrangle for inner integral surface), and  $w_r$  is the corresponding weight for the gauss point.

Then the smoothed Galerkin weak form is formulated finally, in which the smoothing conduction matrix can be obtained as,

$$\bar{\mathbf{K}}_{IJ}^{(k)} = [\bar{\mathbf{B}}_I^{\Omega_k}]^T \mathbf{k} \bar{\mathbf{B}}_J^{\Omega_k} V_k \quad (28)$$

where  $V_k$  is the volume of smoothing domain for node  $k$ .

It can be easily seen from Eq. (28) that the resultant linear system is symmetric and banded (due to the compact supports of PIM shape functions), which implies that the discretized system equations can be solved efficiently.

#### 4. Numerical implementation

A 3D code has been developed in FORTRAN, and a direct Gaussian elimination solver [20] is used in the present 3D NS-PIM code. The code is then used to analyze 3D heat transfer problems. For comparison, the FEM in-house code is also developed to analyze the same problems using the exactly same solver and meshes

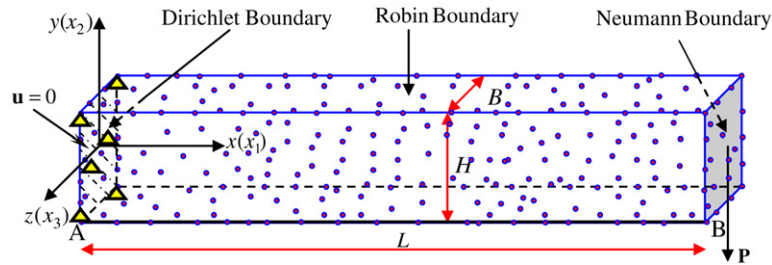


Fig. 3. Discretized model of a 3D conduction beam subjected to Dirichlet, Neumann and Robin boundary conditions on left, right and top surfaces, respectively.

Table 1

Comparison of the solutions of temperature ( $^{\circ}\text{C}$ ) along the AB edge.

$x(\text{m})$	0.01	0.02	0.03	0.04	0.05	0.06	0.07	0.08	0.09	0.10
Reference	286.30	371.77	393.03	398.28	399.58	399.91	400.02	400.20	400.81	403.16
NS-PIM	287.84	372.16	392.88	398.26	399.57	399.90	400.02	400.20	400.80	403.21
FEM	283.47	371.43	392.91	398.25	399.57	399.91	400.02	400.20	400.80	403.11

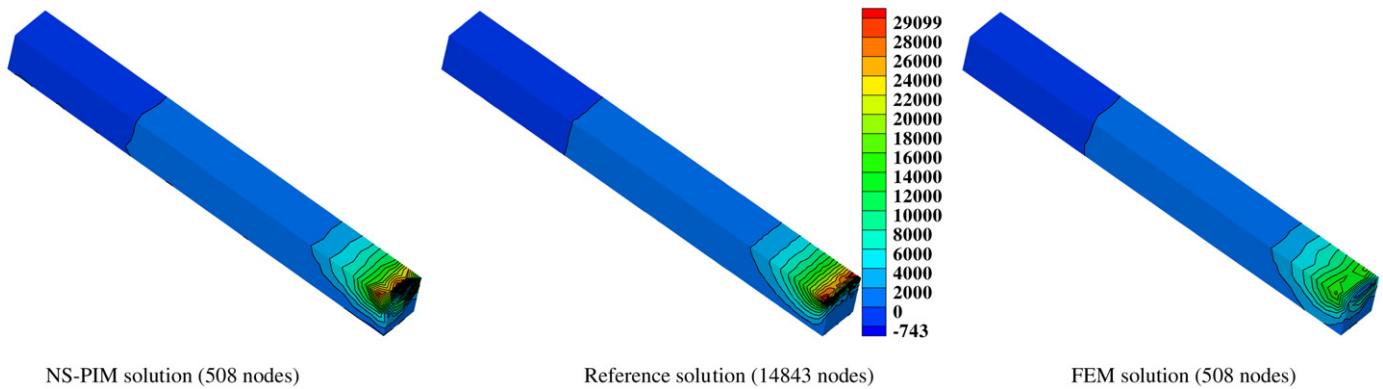


Fig. 4. Comparison of the  $y$  component of temperature gradients.

as the NS-PIM used. As the analytical solutions of these complex problems are not available, reference solution is obtained using the ABAQUS<sup>®</sup>, in which a very fine mesh with high-order elements is adopted. The equivalent energy norm for heat transfer model [1] is defined to evaluate the bound property as

$$U_e = \int_{\Omega} \bar{\mathbf{g}}^T \mathbf{k} \bar{\mathbf{g}} d\Omega \quad (29)$$

where  $\bar{\mathbf{g}}$  is the smoothed temperature gradient in Eq. (24).

#### 4.1. 3D conduction beam

The first example considered here is a 3D conduction beam as shown in Fig. 3. The room temperature  $T_r$  is prescribed onto the left surface, heat flux  $q_r$  continuously enters into the solid from the right surface and heat convection occurs between the top surface and the ambient with a convection coefficient  $h$ . In the computation, the parameters are taken as  $L = 0.1$  m,  $H = 0.01$  m,  $B = 0.01$  m,  $k_1 = 15.0$  W/( $\text{m}^{\circ}\text{C}$ ),  $k_2 = 10.0$  W/( $\text{m}^{\circ}\text{C}$ ),  $k_3 = 5.0$  W/( $\text{m}^{\circ}\text{C}$ ),  $h = 1500$  W/( $\text{m}^2\text{ }^{\circ}\text{C}$ ),  $q_r = -2000$  W/ $\text{m}^2$ ,  $T_r = 0^{\circ}\text{C}$ ,  $Q_v = 0$  W/ $\text{m}^3$  and  $T_a = 400^{\circ}\text{C}$ .

The problem domain is firstly discretized with 508 irregularly distributed nodes, based on which the 4-node tetrahedrons are constructed. For comparison, FEM solutions are also computed using the same tetrahedral mesh. The reference solutions are obtained using a refined mesh of 14 843 irregular nodes.

#### 4.1.1. Temperature

The computed temperatures at the nodes located on the bottom edge (AB edge in Fig. 3) are listed in Table 1, together with linear FEM and reference solutions.

It can be found that, the numerical solutions obtained using the present NS-PIM are in very good agreement with those of the reference ones. This validates our three-dimensional NS-PIM model for heat transfer problems.

#### 4.1.2. Temperature gradients

In many manufacturing processes especially for the high energy density beam manufacturing, large temperature gradient or temperature difference can be generated in solid components and structures, which can induce severe thermal cracks at the most critical locations where the temperature gradient is largest [21]. Therefore, we use maximum error norm to quantify the accuracy of our numerical solutions. Since it is difficult for experimental studies on these types of systems to accurately measure the temperature gradient [22], it is preferred to predict the gradient distribution using numerical means. Fig. 4 presents of the  $y$ -component of temperature gradient solution ( $^{\circ}\text{C}/\text{m}$ ) using the present NS-PIM and FEM, together with the reference solution. It can be clearly observed that the  $y$  component result obtained using the NS-PIM matches well with the reference one. Fig. 5 shows the corresponding temperature gradient contour in the  $z$ -direction.

It is well known that FEM using tetrahedral elements produces constant gradient field within the elements, which can lead to inaccurate results, especially in the high gradient zone. The computed results in Fig. 5 reveal that the present NS-PIM can obtain

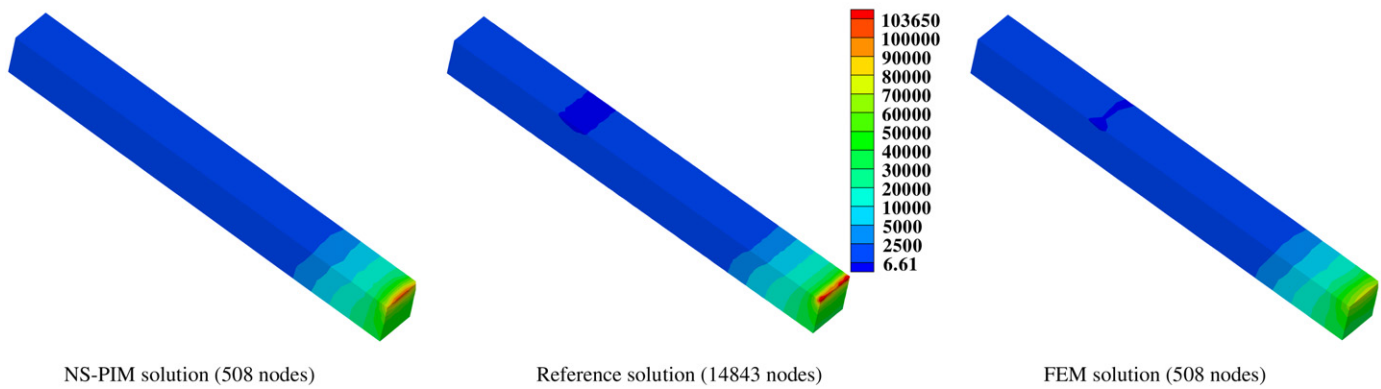


Fig. 5. Comparison of the z component of temperature gradients.

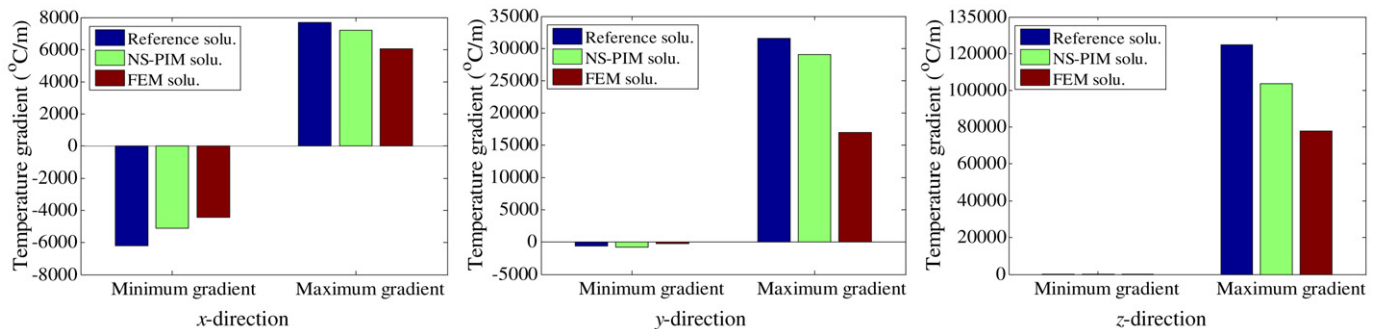


Fig. 6. Comparison of peak temperature gradients between present NS-PIM and linear FEM.

better accuracy than linear FEM especially in the high gradient region.

Fig. 6 presents the peak gradient ( $^{\circ}\text{C}/\text{m}$ ) at the same point in the whole 3D domain. It is shown that the NS-PIM results agree well with the reference solutions, and are more accurate than those obtained from linear FEM using the same mesh. Note that the present NS-PIM formulation is derived from the smoothed Galerkin weak form, in which the smoothed gradient is obtained using Eq. (23). The NS-PIM model so constructed behaves much “softer” compared with the FEM model, and hence produces much more accurate and more smoothing solution in terms of temperature gradient. The similar phenomenon [13,14,18] has also been observed for thermoelasticity and solid mechanics: NS-PIM can obtain higher accuracy on displacement gradients or stresses than the FEM using the same linear mesh.

#### 4.1.3. Solution bound

It is well known that the displacement-based fully compatible FEM model always provides a lower bound in energy form of the exact solution to elastic problems. It is, however, much more difficult to numerically bound the solution from above for complicated heat transfer problems. To present the very important bound property, four NS-PIM models of the conduction beam are built with irregularly distributed nodes (163, 508, 1147 and 2605). Fig. 7 shows the convergence process of the solution in terms of the equivalent energy with the increase of the degree of freedoms (DOF). Both present NS-PIM and FEM are used in this study together with the reference solution obtained using ABAQUS<sup>®</sup> with very fine mesh and high-order elements (14843 nodes).

It can be clearly observed that the equivalent energy of NS-PIM model is larger than that of the reference solution; on the contrary, the energy of FEM model is smaller than the reference value. This finding confirms that the 3D NS-PIM formulation can provide upper bound solution for heat transfer problems [13], which is an important complement to the fully compatible FEM.

## 4.2. An engine pedestal

The following subsection analyzes a real engine pedestal with complex geometries, which is manufactured by the plasma deposition-layered technique [16]. The pedestal part is made of super-alloy material, and detailed dimensions and processing parameters can be found in Ref. [22]. Fig. 8 is the schematics of the engine pedestal.

The CD arc is divided into regularly nine segments to present the temperature. In the computation, complicated boundary conditions are enforced based on Eqs. (4)–(6), respectively. The parameters and conditions used are the same as the 3D conduction beam studied in Section 4.1.

### 4.2.1. Temperature

The problem domain is represented using the background tetrahedral mesh with 754 nodes and the nodal temperatures on the CD arc (shown in Fig. 8) are listed in Table 2, together with linear FEM and reference ones (30222 nodes). It can be observed that numerical results are always larger than linear FEM and reference ones, and linear FEM solutions are the smallest: showing again the upper bound property of the NS-PIM.

### 4.2.2. Temperature gradients

The computed temperature gradients ( $^{\circ}\text{C}/\text{m}$ ) in x-direction are plotted in Fig. 9 in the form of contour lines for both the NS-PIM and linear FEM, together with the reference solution obtained using a very fine mesh (30222 nodes). It can be clearly seen that temperature gradients obtained using the NS-PIM agrees well with the reference ones especially in the high gradient region, and more accurate than that of the FEM.

Fig. 10 shows the comparison of temperature gradients in z-direction. It can be observed again that the computed result obtained using the NS-PIM is more accurate than that obtained from

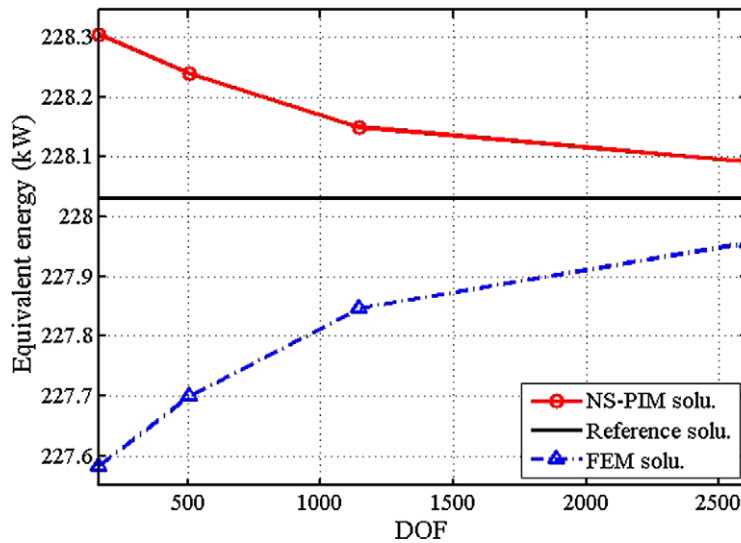


Fig. 7. Upper and lower bound solutions of the 3D conduction beam obtained using the present NS-PIM and linear FEM, respectively.

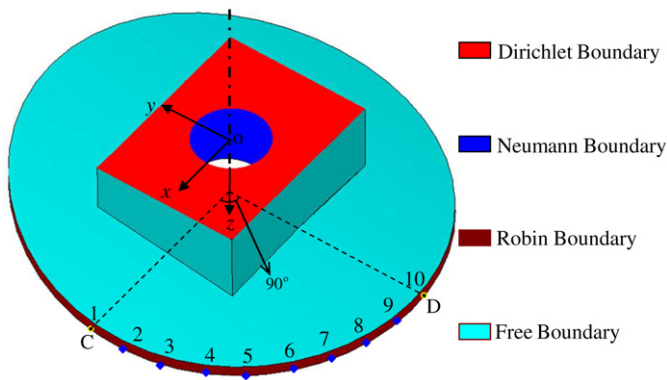


Fig. 8. Illustration of the complex part subjected to Dirichlet, Neumann and Robin conditions on the baseplane, the inner surface of through-hole, the edge surface of the cap plate, respectively.

the linear FEM, and closer to reference one, especially in the high temperature gradient region.

Fig. 11 further demonstrates the accuracy of the gradient solutions ( $^{\circ}\text{C}/\text{m}$ ) at the same point in the 3D domain. It can be clearly seen that computed temperature gradients using the NS-PIM are very close to the reference results, which shows that the present NS-PIM provides more accurate gradient solutions than the linear FEM.

4.2.3. Solution bound

Fig. 7 has shown that the NS-PIM solution (in equivalent energy norm) is larger than the reference solution, and in turn the reference solution is larger than that of the displacement-based FEM. This numerical finding reveals the bound property of the present NS-PIM. To further confirm the upper bound property, four models of this complex problem are generated with irregularly scattered 754, 1389, 2447 and 3287 nodes, respectively. Fig. 12 plots the numerical solutions against the increasing of DOF for NS-PIM and

FEM as well as the reference one obtained using a very fine mesh (irregularly distributed 30 222 nodes).

It can be found that, for this complex 3D engine pedestal, the present NS-PIM again provides an upper bound solution in equivalent energy norm with homogeneous essential boundary conditions ( $T_r = 0$ ), and converges to the reference solution with the increase in DOFs. On the contrary, the FEM solution approaches to the reference solution from below.

Figs. 7 and 12 show that with the increase of DOFs, equivalent energy norm of the FEM model and the present NS-PIM model converges to the reference solution from below and above, respectively. This important property implies also that we can numerically obtain very accurate solutions using a hybrid model of FEM and NS-PIM. More important, engineers can readily verify a numerical solution and conduct the adaptive analysis for solutions of the desired accuracy for complex solid and structures subjected to complicated thermal conditions and loading. Such an analysis can always be done, as long as a FEM mesh can be build.

4.3. Comparison of efficiency

A comparison study on computational efficiency is now performed on the same Dell PC of Inter<sup>®</sup> Pentium (R) CPU 2.80 GHz, 1.00 GB of RAM using models of same DOFs. In order to conduct a thorough study in an efficient manner, we choose to use 2D problems [13]. The MFree2D<sup>®</sup> [3] is therefore used in the tests where a well-coded “bandwidth” solver with one-column storage technique is available. Tables 3 and 4 list respectively, the CPU time required to form the linear system and to solve the resulted system equations, using NS-PIM, FEM and EFG for the same problem of engine pedestal part. It can be found from Tables 3 and 4 that (i) the CPU time is dominated by solving the stiffness matrix of NS-PIM, and the extra CPU time for the smoothing operations performed in Eq. (22), computing the stiffness matrix, and assembling the linear system is very little and negligible; (ii) the CPU time consumed by equation solver in NS-PIM is about 3–4 times more than the

Table 2 Comparison of the solutions of temperature ( $^{\circ}\text{C}$ ) along the CD arc.

Node ID	1	2	3	4	5	6	7	8	9	10
Reference	266.62	277.35	282.46	288.12	293.94	299.55	304.53	308.81	314.54	316.47
NS-PIM	269.89	281.34	285.66	290.89	296.68	302.20	307.16	311.06	316.22	318.74
FEM	262.93	273.46	278.50	284.36	290.31	296.36	301.42	306.23	311.94	313.79

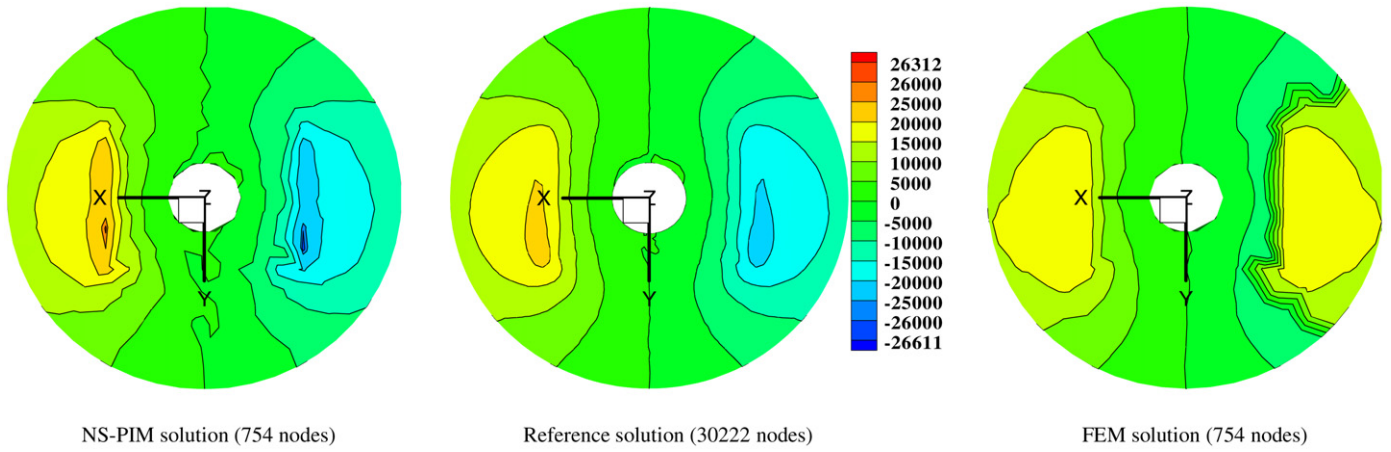


Fig. 9. Comparison of temperature gradients in y-direction.

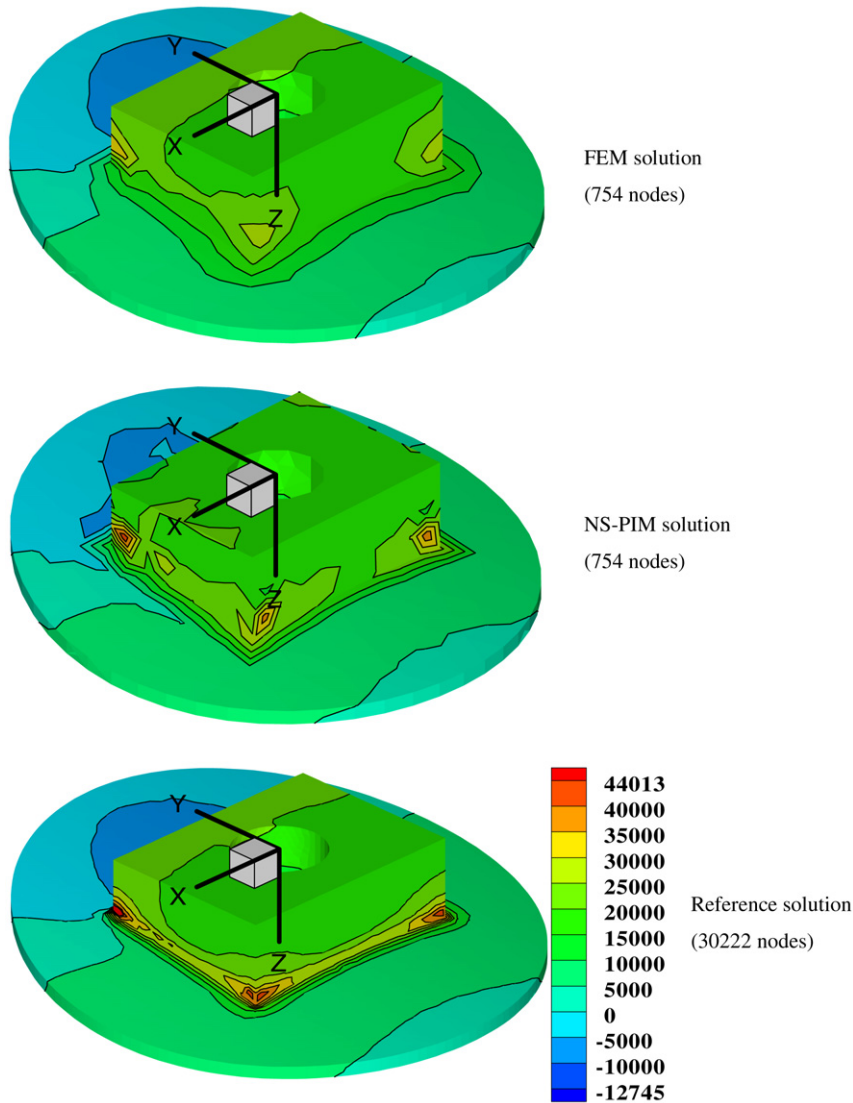


Fig. 10. Comparison of temperature gradient in z-direction.

well-developed FEM, and is nine times faster than the widely-used meshfree EFG [5].

Note that meshfree methods were known [3] to require more CPU time compared to well-developed FEM for models of same

DOFs. This is because more local nodes are used in the formulation resulting in a reduction of the sparsity in the system matrix. On the other hand, methods using meshfree techniques are found having a number of attractive features, such as adaptivity to

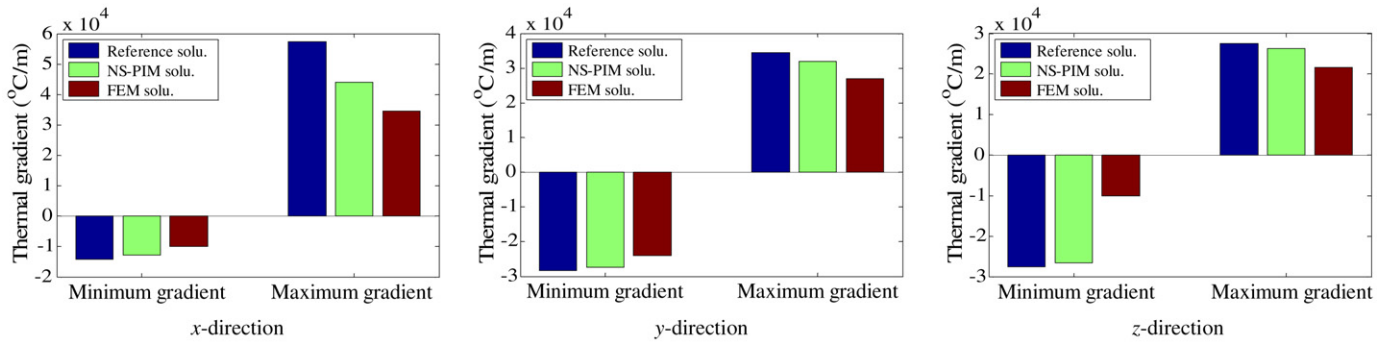


Fig. 11. Comparison of peak temperature gradient for both NS-PIM and linear FEM.

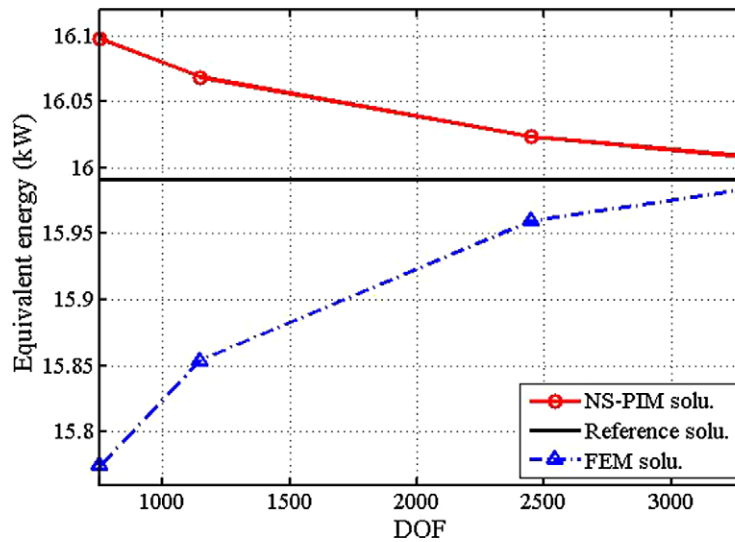


Fig. 12. Upper and lower bound solutions of the 3D engine pedestal obtained using the present NS-PIM and linear FEM, respectively.

Table 3

Comparison of the CPU time (s) to form the linear system.

DOFs	NS-PIM	FEM
7020	0.297	0.267
20922	0.861	0.768
60572	2.643	2.353
88814	4.270	3.622

Table 4

Comparison of the CPU time (s) to solve the resulting equations.

DOFs	NS-PIM	FEM	EFG (Bucket)
7020	0.533	0.156	4.514
20922	5.177	1.331	41.913
60572	41.672	9.314	356.994
88814	87.143	19.22	851.330

mesh distortion [10], convenience in adaptive analysis [23,24], very close-to-exact stiffness [25], and upper bound solutions [14], etc. For NS-PIM, the most significant factor consuming more CPU time is also the less sparsity in the stiffness matrix due to more local nodes used in computing the smoothed strain fields. The bandwidth of an NS-PIM matrix is about twice of that of an FEM model, which results in about 3–4 times more CPU time in solving the equations. This analysis is supported by our numerical test results given in Table 4.

In terms of computational efficiency (CPU time for the same accuracy in energy norm) [26], however, meshfree methods can stand out that depends on method and type of solver used, and

the measure of errors. The NS-PIM was found superior to the FEM even using a full matrix solver with energy norm as error measure, as reported in [18]. This is because more accurate results in temperature gradient and stress [14] can be obtained using NS-PIM with the same number of DOFs. More importantly, the NS-PIM model possesses a “softer” stiffness and can produce upper bound solutions, in contrast to the “overly-stiff” FEM model that produces lower bound solutions. This is confirmed by both solid mechanics problems and heat transfer problems in this work.

## 5. Conclusions

In this work, a NS-PIM is formulated for 3D heat transfer problems with complex geometrics and complicated boundary conditions, using four-node tetrahedrons. The smoothed Galerkin weak form is then used to create the discretized system equations. Problems of actual mechanical parts are analyzed to examine the accuracy, efficiency and upper bound property of the NS-PIM. Several remarks can be made as follows:

1. No derivative of shape functions is required any more due to the use of the gradient smoothing technique, which results in more accurate gradient solutions even using the low-order shape functions, and shape functions used are not globally continuous.
2. For the problems studied in this paper, the NS-PIM can achieve higher accuracy in temperature field and its gradients even in high gradient zone, compared with FEM using the same coarse mesh.

3. For the first time, the upper bound solutions in equivalent energy norm are obtained using the NS-PIM for 3D heat transfer problems with homogeneous boundary conditions. Together with the standard FEM, we now have a simple means to bound the solution for heat transfer problems from both below and above using the same tetrahedral mesh. This can always be done as long as a reasonably fine FEM mesh can be created.
4. In contrast with the conventional FEM, the NS-PIM is more effective to the 3D complex problems, and can efficiently handle complicated boundary conditions of heat transfer problems.

#### Acknowledgements

The National Natural Science Foundation of China under project Nos. 50474053, 50875096 and 50675081 together with the 863 project (No. 2007AA04Z142) are gratefully acknowledged. The authors also give sincerely thanks to the support of Centre for ACES and Singapore-MIT Alliance (SMA), National University of Singapore.

#### References

- [1] O.C. Zienkiewicz, R.L. Taylor, *The Finite Element Method (V1: The Basis)*, 5th ed., Butterworth-Heinemann, Oxford, 2000.
- [2] L.B. Lucy, A numerical approach to testing of the fission hypothesis, *Astron. J.* 8 (1977) 1013–1024.
- [3] G.R. Liu, M.B. Liu, *Smoothed Particle Hydrodynamics—A Meshfree Particle Method*, World Scientific, Singapore, 2003.
- [4] G.R. Liu, *Meshfree Methods: Moving Beyond the Finite Element Method*, CRC Press, Boca Raton, USA, 2002.
- [5] T. Belytschko, Y.Y. Lu, L. Gu, Element-free Galerkin method, *Int. J. Numer. Meth. Engrg.* 37 (1994) 229–256.
- [6] W.K. Liu, S. Jun, Y.F. Zhang, Reproducing kernel particle methods, *Int. J. Numer. Meth. Fluids* 20 (1995) 1081–1106.
- [7] S.N. Atluri, T. Zhu, A new meshless local Petrov–Galerkin (MLPG) approach in computational mechanics, *Comput. Mech.* 22 (1998) 117–127.
- [8] G.R. Liu, Y.T. Gu, A point interpolation method for two-dimensional solids, *Int. J. Numer. Meth. Engrg.* 50 (2001) 937–951.
- [9] G.R. Liu, G.Y. Zhang, Y.Y. Wang, Z.H. Zhong, G.Y. Li, X. Han, A nodal integration technique for meshfree radial point interpolation method (NI-RPIM), *Int. J. Solids Struct.* 44 (2007) 3840–3860.
- [10] G.Y. Zhang, G.R. Liu, T.T. Nguyen, C.X. Song, X. Han, Z.H. Zhong, G.Y. Li, The upper bound property for solid mechanics of the linearly conforming radial point interpolation method (LC-RPIM), *Int. J. Comput. Meth.* 4 (2007) 521–541.
- [11] J.S. Chen, C.T. Wu, S. Yoon, Y. You, A stabilized conforming nodal integration for Galerkin meshfree methods, *Int. J. Numer. Meth. Engrg.* 50 (2001) 435–466.
- [12] G.R. Liu, G.Y. Zhang, K.Y. Dai, Y.Y. Wang, Z.H. Zhong, G.Y. Li, X. Han, A linearly conforming point interpolation method (LC-PIM) for 2D solid mechanics problems, *Int. J. Comput. Meth.* 2 (2005) 645–665.
- [13] S.C. Wu, G.R. Liu, H.O. Zhang, G.Y. Zhang, A node-based smoothed point interpolation method (NS-PIM) for thermoelasticity problems with solution bounds, *Int. J. Heat Mass Tran.* (2008), [10.1016/j.ijheatmasstransfer.2008.09.001](https://doi.org/10.1016/j.ijheatmasstransfer.2008.09.001).
- [14] G.R. Liu, G.Y. Zhang, Upper bound solution to elasticity problems: A unique property of the linearly conforming point interpolation method (LC-PIM), *Int. J. Numer. Meth. Engrg.* 74 (2008) 1128–1161.
- [15] Y. Jaluria, K.E. Torrance, *Computational Heat Transfer*, 2nd ed., Taylor & Francis, London, 2003.
- [16] S.C. Wu, H.O. Zhang, Q. Tang, L. Chen, G.L. Wang, Meshless analysis of the substrate temperature in plasma spraying process, *Int. J. Therm. Sci.* (2008), [doi:10.1016/j.ijthermalsci.2008.06.011](https://doi.org/10.1016/j.ijthermalsci.2008.06.011).
- [17] S.C. Wu, H.O. Zhang, G.L. Wang, Numerical and experimental evaluation of the temperature and stress fields during plasma deposition dieless manufacturing, in: K.P. Rajurkar (Eds.), *Proceeding of the 15th International Symposium on Electro-Machining*, Pittsburgh 2007, pp. 523–528.
- [18] G.R. Liu, A generalized gradient smoothing technique and the smoothed bilinear form for Galerkin formulation of a wide class of computational methods, *Int. J. Comput. Meth.* 5 (2008) 199–236.
- [19] G.R. Liu, A weakened weak ( $W^2$ ) form for a unified formulation of compatible and incompatible displacement methods, *Int. J. Numer. Meth. Engrg.* (2008), submitted for publication.
- [20] S.L. Xu, *FORTRAN Algorithms and Program*, 2nd ed., Tsinghua University Publisher, Beijing, 1995.
- [21] S.C. Wu, G.L. Wang, H.O. Zhang, X.H. Xiong, Plasma deposition dieless manufacturing of turbine parts: thermal stress control and process optimization, *Transactions of the China Welding Institution* 28 (2007) 49–52, 56.
- [22] G.L. Wang, S.C. Wu, H.O. Zhang, Numerical simulation of temperature field on complicated parts during plasma deposition dieless manufacturing, *Transactions of the China Welding Institution* 28 (2007) 49–52.
- [23] G.R. Liu, Z.H. Tu, An adaptive procedure based on background cells for meshfree methods, *Comput. Method Appl. M.* 191 (2002) 1923–1943.
- [24] G.Y. Zhang, G.R. Liu, An efficient adaptive analysis procedure for certified solutions with exact bounds of strain energy for elastic problems, *Finite Elem. Anal. Des.* (2008), [doi:10.1016/j.finel.2008.06.010](https://doi.org/10.1016/j.finel.2008.06.010).
- [25] G.R. Liu, T.T. Nguyen, K.Y. Lam, An edge-based smoothed finite element method (ES-FEM) for static, free and forced vibration analyses of solids, *J. Sound Vib.* (2008), [doi:10.1016/j.jsv.2008.08.027](https://doi.org/10.1016/j.jsv.2008.08.027).
- [26] O.C. Zienkiewicz, J.Z. Zhu, A simple error estimator and adaptive procedure for practical engineering analysis, *Int. J. Numer. Meth. Engrg.* 24 (2008) 1128–1161.